A high-order well-balanced discontinuous Galerkin method for hyperbolic balance laws based on the Gauss-Lobatto quadrature rules*

Ziyao Xu† and Chi-Wang Shu‡

Abstract

In this paper, we develop a high-order well-balanced discontinuous Galerkin method for hyperbolic balance laws based on the Gauss-Lobatto quadrature rules. Important applications of the method include preserving the non-hydrostatic equilibria of shallow water equations with non-flat bottom topography and Euler equations in gravitational fields. The well-balanced property is achieved through two essential components. First, the source term is reformulated in a flux-gradient form in the local reference equilibrium state to mimic the true flux gradient in the balance laws. Consequently, the source term integral is discretized using the same approach as the flux integral at Gauss-Lobatto quadrature points, ensuring that the source term is exactly balanced by the flux in equilibrium states. Our method differs from existing well-balanced DG methods for shallow water equations with non-hydrostatic equilibria, particularly in the aspect that it does not require the decomposition of the source term integral. The effectiveness of our method is demonstrated through ample numerical tests.

Key Words: well-balanced, discontinuous Galerkin, Gauss-Lobatto quadrature, shallow water equations, Euler equations, non-hydrostatic equilibria

1 Introduction

The hyperbolic balance law serves as a fundamental tool for characterizing flow and transport phenomena. In one space dimension, it typically takes the form of

$$\mathbf{u}_t + \mathbf{f}(\mathbf{u})_x = \mathbf{s}(\mathbf{u}, x), \quad x \in \mathbb{R}, t > 0, \tag{1.1}$$

*Research supported by NSF grant DMS-2309249.

†Department of Applied and Computational Mathematics and Statistics, University of Notre Dame, Notre Dame, IN 46556, USA. E-mail: zxu25@nd.edu

‡Division of Applied Mathematics, Brown University, Providence, RI 02912, USA. E-mail: chi-wang_shu@brown.edu

where $\mathbf{u} \in \mathbb{R}^m$ is the vector of balanced quantities, $\mathbf{f}$ the vector of fluxes and $\mathbf{s}$ the vector of source terms. Here and henceforth, letters in boldface font are used to denote quantities of vectors.

Due to the presence of the source term, equation (1.1) often admits non-trivial steady-state solutions, which are time-independent and exactly balance the flux gradient with the source term, i.e. $\mathbf{f}(\mathbf{u}_e(x))_x = \mathbf{s}(\mathbf{u}_e(x), x)$, where $\mathbf{u}_e$ is a steady-state solution. It is desirable to design well-balanced numerical methods that satisfy a discrete version of such a balance, as solutions to many real-world problems are minor deviations from steady states and well-balanced schemes are highly efficient in resolving such small deviations.

A prototypical example of hyperbolic balance laws is the system of shallow water equations, which has been widely used in modeling flows in rivers and coastal areas. The shallow water equations with non-flat bottom topography is written as

$$\begin{cases} h_t + m_x = 0, \\ m_t + \left(hu^2 + \frac{1}{2}gh^2\right)_x = -gh\phi_x, \end{cases} \tag{1.2}$$

where h is the water depth, $m = hu$ is the discharge, u is the velocity, g is the gravitational constant, and ϕ is the prescribed bottom topography.

The shallow water equations (1.2) admit the steady state of lake-at-rest, i.e.

$$u = 0, \quad h + \phi = \text{constant}, \tag{1.3}$$

which is hydrostatic as the velocity is zero. The general non-hydrostatic equilibrium of (1.2) is characterized by

$$m = \text{constant}, \quad \frac{1}{2}u^2 + g(h + \phi) = \text{constant}, \tag{1.4}$$

where m is not necessarily zero, thereby the lake-at-rest (1.3) is a special case of (1.4).

Numerous numerical methods have been developed for the exact preservation of the state of lake-at-rest (1.3), see, e.g. [1, 2, 40, 41, 42, 22, 5, 32], and references therein. It is much more challenging yet highly meaningful to design well-balanced schemes for the non-hydrostatic equilibrium (1.4), which naturally covers the steady state (1.3). We refer the readers to works in the non-exhaustive list [33, 39, 4, 3, 8, 20, 31, 7].

Another important example of the hyperbolic balance laws (1.1) is the system of Euler equations for

compressible gas dynamics, which takes the form of

$$\begin{cases} \rho_t + m_x = 0, \\ m_t + (\rho u^2 + p)_x = -\rho\phi_x, \\ E_t + ((E+p)u)_x = -m\phi_x, \end{cases} \tag{1.5}$$

in gravitational fields, where ρ is the density, $m = \rho u$ is the momentum, u is the velocity, $E = \frac{1}{2}\rho u^2 + \frac{p}{\gamma-1}$ is the total energy per unit volume, p is the pressure, $\gamma > 1$ is the ratio of specific heats, and ϕ is the prescribed potential of the gravitational filed.

The complexity of the Euler equations leads to a richer variety of steady states. Specifically, two types of hydrostatic equilibria have been most thoroughly investigated in previous studies, e.g. [6, 36, 38, 43, 15, 19, 26, 21], which are the isothermal hydrostatic equilibrium,

$$u = 0, \quad \frac{p}{\rho} = \text{constant}, \quad \frac{p}{\rho}\log\rho + \phi = \text{constant}, \tag{1.6}$$

and the polytropic hydrostatic equilibrium,

$$u = 0, \quad \frac{p}{\rho^\gamma} = \text{constant}, \quad \frac{\gamma}{\gamma-1}\frac{p}{\rho} + \phi = \text{constant}. \tag{1.7}$$

The steady state (1.7) is a particular case of the general isentropic equilibria,

$$m = \text{constant}, \quad \frac{p}{\rho^\gamma} = \text{constant}, \quad \frac{1}{2}u^2 + \frac{\gamma}{\gamma-1}\frac{p}{\rho} + \phi = \text{constant}, \tag{1.8}$$

see the studies in [14, 16]. Due to the break of energy conservation, there is generally no corresponding non-hydrostatic equilibria of (1.6).

The objective of this paper is to establish a high-order, well-balanced discontinuous Galerkin (DG) method for the hyperbolic balance law (1.1), which in particular is capable of preserving the general non-hydrostatic equilibria (1.4) and (1.8) for the shallow water equations (1.2) and Euler equations (1.5), respectively. The DG method was first introduced in 1973 by Reed and Hill [35] for solving linear steady-state hyperbolic balance laws, and was later developed into the Runge-Kutta discontinuous Galerkin (RKDG) by Cockburn et al. in a series of papers [9, 10, 11, 12, 13] for nonlinear time-dependent problems. The DG method adopts piecewise polynomials to form its function space and incorporates the concept of numerical fluxes from finite volume methods, making it especially well-suited for solving hyperbolic problems due to its advantages in high-order accuracy, compact stencil, flexibility in geometry, and ease of parallelism. There are many

researches on well-balanced methods within the DG framework. For instance, Xing and Shu developed a high order well-balanced DG method in [41] for hyperbolic balance laws with separable source terms. Subsequently, a more straightforward well-balanced DG for shallow water equations was proposed in [42] based on the hydrostatic reconstruction [1], thanks to the fact that the hydrostatic equilibrium solution lives in the DG space if the bottom topography is projected onto the same space. However, great difficulties arise when designing well-balanced methods for non-hydrostatic equilibria, as the steady-state solutions generally do not live in the space of piecewise polynomials. In [39], the problem was addressed by a recovery technique of local reference equilibrium states and decomposition of the source term into the equilibrium and residual parts. The method has been extended to preserve the moving-water equilibrium of the Ripa model in [4] and the polytropic equilibrium of Euler equations in [26], and incorporated with a modified oscillation free discontinuous Galerkin (OFDG) damping term in [30] to achieve better robustness. More recently, Zhang et al. [45] proposed a new well-balanced DG scheme for the non-hydrostatic equilibria of shallow water equations. The scheme directly approximates the equilibrium variables in the DG space, rather than the conserved ones, resulting in a much cleaner approach yet with increased computational costs in Newton iteration. We also refer to another well-balanced DG method based on global fluxes in [31], as well as related works cited therein.

In this paper, we propose a novel well-balanced DG method for hyperbolic balance laws based on the Gauss-Lobatto quadrature rules. The method is aimed at preserving the non-hydrostatic equilibria of nodal values at the $k+1$ Gauss-Lobatto points, which can be chosen as the degrees of freedom associated with the Lagrange basis for simplicity, in a P^k-DG scheme. The key components of the proposed method are the flux-gradient reformulation of the source terms in local reference equilibrium states and the same approach of discretization for the source term and flux integral at the Gauss-Lobatto points. The special reformulation of the source term is inspired by the treatments in [25, 6, 27], see also [34, 16] for closely related treatment and the survey [18]. A high order well-balanced finite difference WENO scheme has been proposed in our recent work [44] based on the same reformulation. In spirit, our method is very close to the work in [6], which used the nodal DG method to preserve the hydrostatic equilibria of the Euler equations in the gravitational fields.

The remaining of the paper is organized as follows. In Section 2, we review some important properties of the steady states of the shallow water equations and Euler equations. Consequently, the well-balanced DG scheme is established in Section 3 for these equations. The good performance of the scheme is validated in

Section 4 by ample numerical tests. Finally, we end up with some concluding remarks in Section 5.

2 Steady states of the shallow water equations and Euler equations

In this section, we review some properties of the non-hydrostatic equilibria of the shallow water equations and Euler equations, and introduce necessary definitions to facilitate the construction of our well-balanced DG method.

2.1 The shallow water equations with non-flat bottom topography

For the shallow water equations (1.2), we introduce the vector of equilibrium variables

$$\mathbf{v} = (m, Q)^T, \quad \text{where } Q = \frac{1}{2}u^2 + g(h+\phi). \tag{2.1}$$

The vector is constant in the non-hydrostatic equilibria (1.4). Moreover, we denote the mapping from the vector of conserved variables $\mathbf{u} = (h, m)^T$ to equilibrium ones by $\mathbf{v} = V(\mathbf{u}, \phi)$. Its inverse mapping is denoted by $\mathbf{u} = U(\mathbf{v}, \phi)$. If $\mathbf{u}_e$ is an equilibrium state satisfying (1.4), then $\mathbf{u}_e(x) = U(\mathbf{v}_e, \phi(x))$ for the constant $\mathbf{v}_e = V(\mathbf{u}_e(x), \phi(x))$.

For the calculation of $U(\mathbf{v}, \phi)$, we introduce the Froude number

$$\mathrm{Fr} = \frac{|u|}{c}, \quad \text{where } c = \sqrt{gh}. \tag{2.2}$$

The flow regimes of $\mathbf{u}$ are classified as subcritical, critical or supercritical if $\mathrm{Fr} < 1, = 1$ or > 1. In each flow regime, the water depth h is uniquely determined by the formula of trigonometric solution of cubic equation [24, 20],

$$h(m, Q, \phi) = \frac{Q - g\phi}{3g}\left(1 + \cos(\frac{\theta}{3}) - \sqrt{3}\sigma\sin(\frac{\theta}{3})\right), \tag{2.3}$$

where $\theta = \arccos\left(\frac{27}{4}\frac{g^2m^2}{(Q-g\phi)^3} - 1\right)$ and $\sigma = \mathrm{sign}(\text{Fr-1})$, if the equilibrium variables m, Q are given with $Q - g\phi \geq \frac{3}{2}(g|m|)^{\frac{2}{3}}$. For more properties of the equilibrium variables and the mapping $U(\mathbf{v}, \phi)$, we refer the readers to [33].

2.2 The Euler equations in gravitational fields

For the Euler equations (1.5), we introduce the vector of equilibrium variables

$$\mathbf{v} = (m, s, Q)^T, \quad \text{where } s = \frac{p}{\rho^\gamma}, Q = \frac{1}{2}u^2 + \frac{\gamma s}{\gamma - 1}\rho^{\gamma-1} + \phi. \tag{2.4}$$

The vector is constant in the isentropic non-hydrostatic equilibria (1.8). Similarly, we denote the mapping from the vector of conserved variables $\mathbf{u} = (\rho, m, E)^T$ to equilibrium ones by $\mathbf{v} = V(\mathbf{u}, \phi)$. Its inverse mapping is denoted by $\mathbf{u} = U(\mathbf{v}, \phi)$. If $\mathbf{u}_e$ is an equilibrium state satisfying (1.8), then $\mathbf{u}_e(x) = U(\mathbf{v}_e, \phi(x))$ for the constant $\mathbf{v}_e = V(\mathbf{u}_e(x), \phi(x))$.

For the calculation of $U(\mathbf{v}, \phi)$, we introduce the Mach number

$$\text{Mach} = \frac{|u|}{c}, \quad \text{where } c = \sqrt{\gamma p/\rho}. \tag{2.5}$$

The flow regimes of $\mathbf{u}$ are classified as subcritical, critical or supercritical if Mach $< 1, = 1$ or > 1. In each flow regime, the density ρ is uniquely determined by the equation

$$\frac{1}{2}\frac{m^2}{\rho^2} + \frac{\gamma s}{\gamma - 1}\rho^{\gamma-1} + \phi = Q, \tag{2.6}$$

if the equilibrium variables m, s, Q are given with $Q - \phi \geq \left(\frac{1}{2} + \frac{1}{\gamma-1}\right)(\gamma s)^{\frac{2}{\gamma+1}} |m|^{\frac{2(\gamma-1)}{\gamma+1}}$. In practice, we can use Newton iteration to calculate ρ from (2.6) and obtain $E = \frac{1}{2}\frac{m^2}{\rho} + \frac{s\rho^\gamma}{\gamma-1}$ consequently. For more properties of the equilibrium variables and mapping $U(\mathbf{v}, \phi)$, we refer to [16].

3 The well-balanced discontinuous Galerkin method

In this section, we establish the well-balanced DG method for the shallow water equations (1.2) and Euler equations (1.5) in a unified framework, and give the proof of its well-balanced property.

3.1 Notations

We first introduce the notations to be used throughout this section. Consider the domain $\Omega = [a, b] \subset \mathbb{R}$, we take the partition $a = x_{\frac{1}{2}} < x_{\frac{3}{2}} < \cdots < x_{N+\frac{1}{2}} = b$, and denote the j-th cell by $I_j = [x_{j-\frac{1}{2}}, x_{j+\frac{1}{2}}]$ with size $\Delta x_j = x_{j+\frac{1}{2}} - x_{j-\frac{1}{2}}$, for $j = 1, 2, \ldots, N$.

The function space of the P^k-DG scheme is defined as

$$W_h^k = \{w \in L^2([a, b]) : w|_{I_j} \in P^k(I_j), j = 1, 2, \ldots, N\}, \tag{3.1}$$

where $P^k(I)$ denotes the space of polynomials of order no greater than k on the interval I. Since $w \in W_h^k$ are piecewise polynomials with possible discontinuities at interfaces, we define the left/right limits at $x_{j+\frac{1}{2}}$ by $w^{\pm}_{j+\frac{1}{2}} = \lim_{\epsilon\to 0^+} w(x_{j+\frac{1}{2}} \pm \epsilon)$. We also denote $\mathbf{W}_h^k = \left[W_h^k\right]^m$ and $\mathbf{w}^{\pm}_{j+\frac{1}{2}} = \lim_{\epsilon\to 0^+} \mathbf{w}(x_{j+\frac{1}{2}} \pm \epsilon)$ for $\mathbf{w} \in \mathbf{W}_h^k$ as the corresponding vector version of the function space and left/right limits.

To establish the well-balanced DG method, we adopt the $(k+1)$-point Gauss-Lobatto quadrature rule in the P^k-DG scheme, and denote the quadrature of a continuous function g on I_j by $\fint_{I_j} g dx = \Delta x_j \sum_{i=1}^{k+1} \omega_i g(x_i^j)$ to distinguish it from the exact integral $\int_{I_j} g dx$, where $\{x_i^j\}_{i=1}^{k+1}$ and $\{\omega_i\}_{i=1}^{k+1}$ are the Gauss-Lobatto quadrature points (on I_j) and weights, respectively. Note that $x_1^j = x_{j-\frac{1}{2}}$ and $x_{k+1}^j = x_{j+\frac{1}{2}}$, which is important for the scheme to achieve the well-balanced property. We denote by $\mathcal{I}^j[\cdot]$ the Lagrange interpolation operator at the Gauss-Lobatto points on I_j, i.e. $\mathcal{I}^j[g] \in P^k(I_j)$ with $\mathcal{I}^j[g](x_i^j) = g(x_i^j)$ for $i = 1, \ldots, k+1$. For convenience, we write the shortened notation $\mathcal{I}[g]$ for $\mathcal{I}^j[g]$, if the cell j is clear from the context.

3.2 The well-balanced DG scheme

To construct the scheme, we reformulate the hyperbolic balance law (1.1) on I_j as follows [18],

$$\mathbf{u}_t + \mathbf{f}(\mathbf{u})_x = \frac{\mathbf{s}(\mathbf{u}, x)}{\mathbf{s}(\mathbf{u}_e^j, x)} \mathbf{f}(\mathbf{u}_e^j)_x, \tag{3.2}$$

where $\mathbf{u}_e^j$ is a local reference equilibrium state satisfying $\mathbf{f}(\mathbf{u}_e^j(x))_x = \mathbf{s}(\mathbf{u}_e^j(x), x)$ on I_j, whose definition is provided below, and the operations in the source term is understood component-wisely and equal to one in the case of $\frac{0}{0}$.

The well-balanced DG scheme based on the reformulation (3.2) is given as follows: Find $\mathbf{U}(t) \in \mathbf{W}_h^k$, such that, $\forall \mathbf{w} \in \mathbf{W}_h^k$,

$$\int_{I_j} \mathbf{U}_t \cdot \mathbf{w} dx = \fint_{I_j} \mathbf{f}(\mathbf{U}) \cdot \mathbf{w}_x dx - \hat{\mathbf{f}}^l_{j+\frac{1}{2}} \cdot \mathbf{w}^-_{j+\frac{1}{2}} + \hat{\mathbf{f}}^r_{j-\frac{1}{2}} \cdot \mathbf{w}^+_{j-\frac{1}{2}} + \fint_{I_j} \frac{\mathbf{s}(\mathbf{U}, x)}{\mathbf{s}(\mathbf{u}_e^j, x)} \partial_x \left(\mathcal{I}\left[\mathbf{f}(\mathbf{u}_e^j)\right] \right) \cdot \mathbf{w} dx, \tag{3.3}$$

for $j = 1, 2, \ldots, N$, where

$$\begin{aligned} \hat{\mathbf{f}}^l_{j+\frac{1}{2}} &= \mathbf{F}\left(\mathbf{U}^{*,-}_{j+\frac{1}{2}}, \mathbf{U}^{*,+}_{j+\frac{1}{2}}\right) - \mathbf{f}(\mathbf{U}^{*,-}_{j+\frac{1}{2}}) + \mathbf{f}(\mathbf{U}^-_{j+\frac{1}{2}}), \\ \hat{\mathbf{f}}^r_{j-\frac{1}{2}} &= \mathbf{F}\left(\mathbf{U}^{*,-}_{j-\frac{1}{2}}, \mathbf{U}^{*,+}_{j-\frac{1}{2}}\right) - \mathbf{f}(\mathbf{U}^{*,+}_{j-\frac{1}{2}}) + \mathbf{f}(\mathbf{U}^+_{j-\frac{1}{2}}), \end{aligned} \tag{3.4}$$

are numerical fluxes based on the flux function $\mathbf{F}(\cdot, \cdot)$, e.g. the Lax-Friedrichs flux

$$\mathbf{F}(\mathbf{U}^-, \mathbf{U}^+) = \frac{1}{2}\left(\mathbf{f}(\mathbf{U}^-) + \mathbf{f}(\mathbf{U}^+) - \alpha\left(\mathbf{U}^+ - \mathbf{U}^-\right)\right), \tag{3.5}$$

with $\alpha = \max_{\mathbf{U}}\{|\lambda_1(\mathbf{U})|, \ldots, |\lambda_m(\mathbf{U})|\}$ and λ_i the eigenvalues of the system (1.1), and the generalized hydrostatic reconstruction [1, 45] $\mathbf{U}^{*,\pm}_{j+\frac{1}{2}}$ are defined as

$$\mathbf{U}^{*,\pm}_{j+\frac{1}{2}} = U(\mathbf{V}^{\pm}_{j+\frac{1}{2}}, \phi^*_{j+\frac{1}{2}}), \tag{3.6}$$

with $\mathbf{V}^{\pm}_{j+\frac{1}{2}} = V(\mathbf{U}^{\pm}_{j+\frac{1}{2}}, \phi^{\pm}_{j+\frac{1}{2}})$ and $\phi^{*}_{j+\frac{1}{2}} = \min(\phi^{-}_{j+\frac{1}{2}}, \phi^{+}_{j+\frac{1}{2}})$. The Lagrange basis at Gauss-Lobatto points is particularly suitable for the computation of the scheme, and the same quadrature can also be used for the left-hand side, which results in the nodal formulation [17].

The local reference equilibrium state $\mathbf{u}^j_e$ is defined as follows,

$$\mathbf{u}^j_e(x) = U(\mathbf{V}^j_e, \phi(x)), \quad x \in I_j, \tag{3.7}$$

where $\mathbf{V}^j_e = V(\mathbf{U}(x^j_\ell), \phi(x^j_\ell))$, $\ell = \arg\max_{1\le i\le k+1} \phi(x^j_i)$, and the values of piecewise functions at x^j_1 and x^j_{k+1} are understood as inside I_j for the time being. With such a choice of ℓ, $\mathbf{u}^j_e$ is always well-defined on I_j.

Remark 3.1. *For the Euler equations, we have* $\mathbf{s}(\mathbf{u}, x) = (0, -\rho\phi_x, -m\phi_x)^T, \mathbf{s}(\mathbf{u}^j_e, x) = (0, -\rho^j_e\phi_x, -m^j_e\phi_x)^T$, *and* $\mathbf{f}(\mathbf{u}^j_e) = (m^j_e, \frac{(m^j_e)^2}{\rho^j_e} + p^j_e, (E^j_e + p^j_e)\frac{m^j_e}{\rho^j_e})$, *where* m^j_e *is a constant. After cancellations, the reformulation of the source term in* (3.2) *can be simplified as* $\left(0, \frac{\rho}{\rho^j_e}, m\right)^T \times \partial_x(0, \frac{(m^j_e)^2}{\rho^j_e} + p^j_e, (E^j_e + p^j_e)\frac{1}{\rho^j_e})^T$, *where the operations are understood component-wisely. Similarly, for the shallow water equations, the reformulation of the source term in* (3.2) *can be simplified as* $\left(0, \frac{h}{h^j_e}\right)^T \times \partial_x(0, \frac{(m^j_e)^2}{h^j_e} + \frac{1}{2}g(h^j_e)^2)^T$.

3.3 The well-balanced property

The scheme (3.3) is well-balanced in the sense that, if its solution $\mathbf{U}$ is in equilibrium at all Gauss-Lobatto points $\{x^j_i\}_{i=1}^{k+1}, j = 1, 2, \ldots, N$, then the right-hand side is zero, which can be stated as the following theorem.

Theorem 3.1. *If* $\mathbf{U} \in \mathbf{W}^k_h$ *satisfies* $\mathbf{U}|_{I_j} = \mathcal{I}^j[\mathbf{u}_e], j = 1, \ldots, N$, *for an equilibrium state* $\mathbf{u}_e$ *of* (1.1), *then the right-hand side of* (3.3) *is zero.*

Proof. We denote by $\mathbf{V}^j_i = V(\mathbf{U}(x^j_i), \phi(x^j_i))$ for $i = 1, \ldots, k+1, j = 1, \ldots, N$. Since $\mathbf{U}(x^j_i) = \mathbf{u}_e(x^j_i)$ and $V(\mathbf{u}_e(x), \phi(x)) \equiv \mathbf{v}_e$, we have $\mathbf{V}^j_i \equiv \mathbf{v}_e$, $\forall i, j$, where $\mathbf{v}_e$ is a constant. Therefore, $\mathbf{U}^{*,-}_{j+\frac{1}{2}} = U(\mathbf{v}_e, \phi^*_{j+\frac{1}{2}}) = \mathbf{U}^{*,+}_{j+\frac{1}{2}}$, which implies $\hat{\mathbf{f}}^l_{j+\frac{1}{2}} = \mathbf{f}(\mathbf{U}^-_{j+\frac{1}{2}})$ and $\hat{\mathbf{f}}^r_{j-\frac{1}{2}} = \mathbf{f}(\mathbf{U}^+_{j-\frac{1}{2}})$ from the consistency of $\mathbf{F}(\cdot,\cdot)$. Moreover, by the definition (3.7), we have $\mathbf{u}^j_e(x) = \mathbf{u}_e, j = 1, \ldots, N$.

Consequently, the right-hand side of (3.3) is

$$\begin{aligned} RHS_j &= \fint_{I_j} \mathbf{f}(\mathbf{U}) \cdot \mathbf{w}_x dx - \mathbf{f}(\mathbf{U}^-_{j+\frac{1}{2}}) \cdot \mathbf{w}^-_{j+\frac{1}{2}} + \mathbf{f}(\mathbf{U}^+_{j-\frac{1}{2}}) \cdot \mathbf{w}^+_{j-\frac{1}{2}} + \fint_{I_j} \partial_x \left(\mathcal{I}[\mathbf{f}(\mathbf{U})]\right) \cdot \mathbf{w} dx \\ &= \int_{I_j} \mathcal{I}[\mathbf{f}(\mathbf{U})] \cdot \mathbf{w}_x dx - \mathbf{f}(\mathbf{U}^-_{j+\frac{1}{2}}) \cdot \mathbf{w}^-_{j+\frac{1}{2}} + \mathbf{f}(\mathbf{U}^+_{j-\frac{1}{2}}) \cdot \mathbf{w}^+_{j-\frac{1}{2}} + \int_{I_j} \partial_x \left(\mathcal{I}[\mathbf{f}(\mathbf{U})]\right) \cdot \mathbf{w} dx \\ &= 0, \end{aligned}$$

where the second equality is because the $(k+1)$-point Gauss-Lobatto quadrature rule is exact for polynomials of degree no greater than $2k-1$, and the last equality is a consequence of integration by parts. □

Remark 3.2. *By Theorem 3.1, if the initial condition* $\mathbf{u}_0$ *of equation* (1.1) *is in equilibrium, which is generally non-polynomial, we should take the initial condition* $\mathbf{U}_0$ *of scheme* (3.3) *by the Lagrange interpolation* $\mathbf{U}_0 = \mathcal{I}[\mathbf{u}_0]$ *to preserve the equilibrium exactly.*

3.4 An extra damping term

Following [28], we add an extra oscillation free discontinuous Galerkin (OFDG) damping term to the scheme (3.3) to control the spurious oscillations without breaking the well-balanced property.

The well-balanced OFDG scheme is given as follows: Find $\mathbf{U}(t) \in \mathbf{W}_h^k$, such that, $\forall \mathbf{w} \in \mathbf{W}_h^k$,

$$LHS_j = RHS_j - \sum_{\ell=0}^{k} \frac{\sigma_j^\ell(\mathbf{U})}{\Delta x_j} \int_{I_j} \left(\mathbf{U}_r^j - P_h^{\ell-1}\mathbf{U}_r^j\right) \cdot \mathbf{w} dx, \tag{3.8}$$

for $j = 1, 2, \ldots, N$, where LHS_j and RHS_j are the original left-hand and right-hand sides of (3.3), respectively, and $\mathbf{U}_r^j = \mathbf{U}|_{I_j} - \mathcal{I}\left[\mathbf{u}_e^j\right]$ is the residual of equilibrium state, $P_h^{\ell-1}, \ell \geq 1$ is the standard component-wise L^2-projection on $P^{\ell-1}(I_j)$ and $P_h^{-1} = P_h^0$. The damping coefficients $\sigma_j^\ell(\mathbf{U})$ are constructed in exactly the same way as [28] and [29] for the shallow water equations and Euler equations, respectively. Since $\mathbf{U}|_{I_j} = \mathcal{I}[\mathbf{u}_e^j]$ in equilibrium, it is clear that the OFDG damping term does not destroy the well-balanced property of (3.3).

Beside the OFDG method, appropriate slope limiters, e.g., [4, 45], may also be used to control the oscillation without affecting the well-balanced property.

4 Numerical tests

In this section, we test the performance of the proposed well-balanced DG scheme (3.8) for the shallow water equations and Euler equations, with the classic fourth order Runge-Kutta time discretization. We take the step size of time as $\Delta t = \frac{\text{CFL}}{||\,|u|+c\,||_{L^\infty(\Omega)}} \Delta x$, where Δx is the minimum cell length of mesh and CFL is a constant taken as 0.1 in the tests if not otherwise stated. The gravitational constant in the shallow water equations are taken as $g = 9.812$ in all tests. To save space, we only show the results of P^2-DG scheme in the well-balanced tests. All numerical examples in this section are classic. We refer the readers to the results of other methods, e.g. [8, 16, 23, 28, 33, 37, 43, 45], for comparison.

4.1 The shallow water equations

Example 4.1. ***Accuracy test***

In this example, we test the accuracy of the proposed well-balanced DG method for the shallow water equations with a smooth bottom.

The bottom topography and initial conditions of the problem are given by

$$\phi(x) = \sin^2(\pi x), \quad h(x,0) = 5 + e^{\cos(2\pi x)}, \quad m(x,0) = \sin(\cos(2\pi x)). \tag{4.1}$$

The computational domain is $\Omega = [0,1]$ *with periodic boundary condition.*

Since the analytical solution of the problem is not available, we calculate the reference solution using the ninth-order WENO finite difference scheme on $N = 6400$ *grid. The* L^1 *errors and orders of convergence of* h *and* m *with* N *uniform cells are listed in Table 1, at the terminal time* $T = 0.1$ *before shock formation. We can clearly observe high order convergence rates for* P^1*,* P^2 *and* P^3*-DG methods from the table.*

Example 4.2. ***Well-balanced test for a smooth bottom topography***

In this example, we test the well-balanced property of our scheme for a smooth bottom in different flow regimes.

The bottom topography of the problem is given by

$$\phi(x) = \begin{cases} 0.2 - 0.05(x-10)^2, & 8 \le x \le 12, \\ 0, & \textit{otherwise}, \end{cases} \tag{4.2}$$

on the domain $\Omega = [0,25]$*. We impose the boundary conditions by keeping the values on boundaries constant and equal to the initial conditions.*

Below, we consider four non-hydrostatic equilibria in different flow regimes:

(a) Subcritical flow:

$$m(x,0) = 4.42, \quad Q(x,0) = 22.06605, \quad \textit{with} \quad Fr(x,0) < 1.$$

(b) Supercritical flow:

$$m(x,0) = 24, \quad Q(x,0) = 91.624, \quad \textit{with} \quad Fr(x,0) > 1.$$

		h		m	
P^k-DG	N	L^1 error	order	L^1 error	order
	100	2.41E-03	-	1.63E-02	-
	200	3.75E-04	2.68	2.56E-03	2.67
$k=1$	400	6.68E-05	2.49	4.60E-04	2.48
	800	1.17E-05	2.51	7.96E-05	2.53
	1600	2.29E-06	2.36	1.53E-05	2.38
	100	9.19E-05	-	7.74E-04	-
	200	5.60E-06	4.04	4.73E-05	4.03
$k=2$	400	3.69E-07	3.93	3.09E-06	3.94
	800	2.92E-08	3.66	2.44E-07	3.66
	1600	2.82E-09	3.37	2.35E-08	3.38
	100	5.07E-06	-	4.26E-05	-
	200	2.28E-07	4.47	1.94E-06	4.46
$k=3$	400	9.19E-09	4.63	7.85E-08	4.62
	800	3.43E-10	4.74	2.94E-09	4.74
	1600	1.40E-11	4.62	1.23E-10	4.57

Table 1: L^1 errors and orders of convergence in the accuracy test 4.1 for the shallow water equations. Reference solution is obtained by WENO-9 on $N = 6400$ grid.

(c) Transcritical flow without shock:

$$m(x,0) = 1.53, \quad Q(x,0) = \frac{3}{2}\left(9.812 \times 1.53\right)^{\frac{2}{3}} + 9.812 \times 0.2,$$
$$\textit{with} \quad \begin{cases} Fr(x,0) < 1, & x < 10, \\ Fr(x,0) > 1, & x > 10. \end{cases}$$

(d) Transcritical flow with a stationary shock:

$$m(x,0) = 0.18, \quad Q(x,0) = \begin{cases} \frac{3}{2}\left(9.812 \times 0.18\right)^{\frac{2}{3}} + 9.812 \times 0.2, & x \le 11.665504281554291, \\ \frac{0.18^2}{2 \times 0.33^2} + 9.812 \times 0.33, & \textit{otherwise}, \end{cases}$$
$$\textit{with} \quad \begin{cases} Fr(x,0) < 1, & x < 10 \ \textit{or} \ x > 11.665504281554291, \\ Fr(x,0) > 1, & 10 < x < 11.665504281554291. \end{cases}$$

We compute the solutions of case (a), (b), (c) and (d) on $N = 200$ *meshes up to* $T = 10$*. The cells are uniform for the first three cases. Due to the appearance of a shock at* $x = 11.665504281554291$ *in the last case, we use the Roe flux as in [45] and partition* 100 *uniform cells for the regions on the left and right sides of the shock, respectively, such that the shock locates exactly at a cell interface of the mesh.*

The L^1 *and* L^∞ *errors of the numerical solutions compared with the solution at initial time are listed in Table 2, from which we can observe that the errors are in the round-off level, which confirms the well-balanced property of the scheme.*

	h		m	
Case	L^1 error	L^∞ error	L^1 error	L^∞ error
(a)	5.55E-17	6.66E-16	4.26E-16	2.66E-15
(b)	1.69E-13	3.73E-14	1.52E-12	3.87E-13
(c)	1.43E-14	4.72E-15	2.89E-14	1.02E-14
(d)	6.54E-15	1.28E-15	1.50E-14	2.55E-15

Table 2: L^1 and L^∞ errors for different cases in the well-balanced test 4.2 with $N = 200$ at $T = 10$. Continuous bottom topography. Case (a): subcritical flow; Case (b): supercritical flow; Case (c): transcritical flow without shock; Case (d): transcritical flow with a stationary shock.

Example 4.3. ***Well-balanced test for a discontinuous bottom topography***

In this example, we test the well-balanced property of the proposed scheme for a discontinuous bottom in different flow regimes.

The bottom topography of the problem is given by

$$\phi(x) = \begin{cases} 0.2, & 8 \le x \le 12, \\ 0, & otherwise, \end{cases} \tag{4.3}$$

on the domain $\Omega = [0, 25]$. *We impose the boundary conditions by keeping the values on boundaries constant and equal to the initial conditions.*

Below, we consider three non-hydrostatic equilibria in different flow regimes:

(a) Subcritical flow: The settings are the same as case (a) in Example 4.2.

(b) Supercritical flow: The settings are the same as case (b) in Example 4.2.

(c) Transcritical flow:

$$m(x,0) = 1.53, \quad Q(x,0) = \frac{3}{2}\left(9.812 \times 1.53\right)^{\frac{2}{3}} + 9.812 \times 0.2,$$

$$with \quad \begin{cases} Fr(x,0) < 1, & x < 8, \\ Fr(x,0) = 1, & 8 \le x \le 12, \\ Fr(x,0) > 1, & x > 12. \end{cases}$$

We compute the solutions of case (a), (b) and (c) on $N = 200$ *uniform meshes up to* $T = 10$.

The L^1 *and* L^∞ *errors of the numerical solutions compared with the solution at initial time are listed in Table 3, from which we can observe that the errors are in the round-off level, which verifies the well-balanced property of the scheme.*

Example 4.4. ***Small perturbation of steady states for the smooth bottom***

In this example, we test the capability of the proposed scheme to capture small perturbations of equilibria for smooth bottom topography. We add $\delta = 0.05$ *in the region* $x \in [5.75, 6.25]$ *on top of the initial water depth of case (a), (b), (c) and (d) in Example 4.2, and compute the solutions up to* $T = 1.5, 1.0, 1.5$ *and* 3.0, *respectively.*

We show the numerical results with locally zoomed boxes in Figure 1, from which we can see the small perturbations are captured very well.

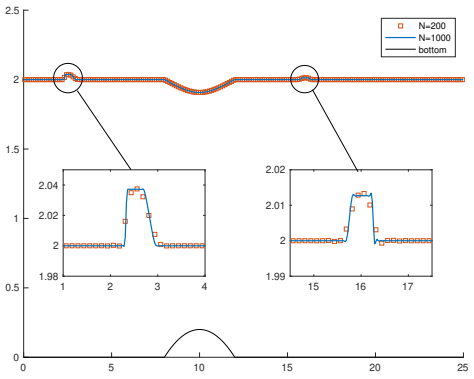

(a) Case (a)

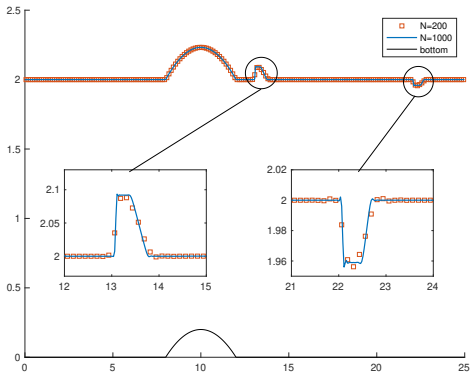

(b) Case (b)

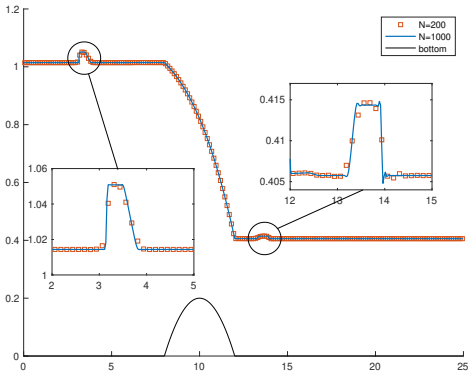

(c) Case (c)

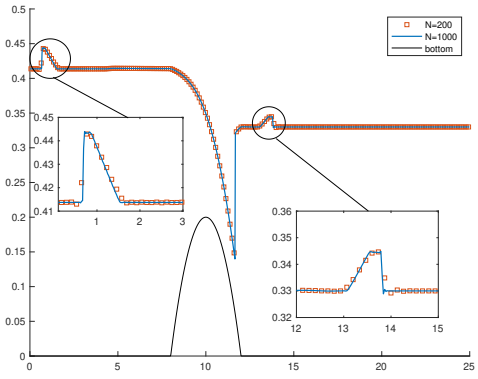

(d) Case (d)

Figure 1: Surface level $h + \phi$ and bottom in the test of small perturbations of steady states for smooth bottom in Example 4.4.

	h		m	
Case	L^1 error	L^∞ error	L^1 error	L^∞ error
(a)	1.85E-17	4.44E-16	0	0
(b)	1.75E-13	2.89E-14	1.60E-12	3.06E-13
(c)	1.05E-14	2.89E-15	2.00E-14	7.55E-15

Table 3: L^1 and L^∞ errors for different cases in the well-balanced test 4.3 with $N = 200$ at $T = 10$. Discontinuous bottom topography. Case (a): subcritical flow; Case (b): supercritical flow; Case (c): transcritical flow.

Example 4.5. ***Small perturbation of steady states for the discontinuous bottom***

In this example, we test the capability of the proposed scheme to capture small perturbations of equilibria for discontinuous bottom topography. We add $\delta = 0.05$ *in the region* $x \in [5.75, 6.25]$ *on top of the initial water depth of case (a), (b) and (c) in Example 4.3, and compute the solutions up to* $T = 1.5, 1.0,$ *and* 1.5*, respectively.*

We show the numerical results with locally zoomed boxes in Figure 2, from which we can see that the small perturbations are captured very well.

Example 4.6. ***Dam breaking over a rectangular bump***

In this example, we test the dam breaking over a rectangular bump.

The bottom topography and initial conditions of the problem are given by

$$b(x) = \begin{cases} 8, & |x - 750| \le 187.5, \\ 0, & \textit{otherwise}, \end{cases} \qquad h(x,0) = \begin{cases} 20 - b(x), & x \le 750, \\ 15 - b(x), & \textit{otherwise}, \end{cases} \qquad m(x,0) = 0.$$

The computational domain is $\Omega = [0, 1500]$*. We impose the boundary conditions by keeping the boundary values constant and equal to the initial conditions.*

We compute the solution of the DG scheme on $N = 200, 400$ *uniform meshes with CFL* $= 0.05$*, and draw the cell averages of surface level* $h + \phi$ *at* $T = 15, 60$ *in Figure 3. The reference solutions in the figure are given by WENO finite difference scheme on* $N = 6400$ *grid. The results exhibit good resolution and essentially oscillation free fashion as in [30].*

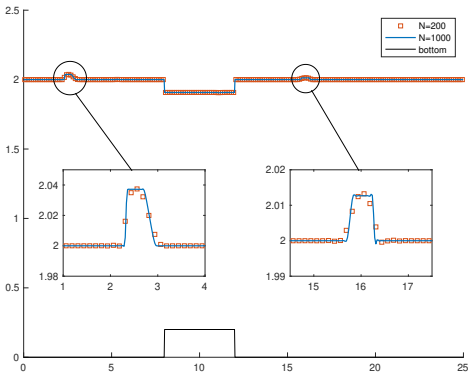

(a) Case (a)

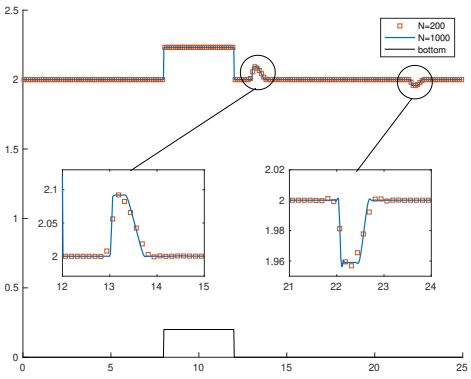

(b) Case (b)

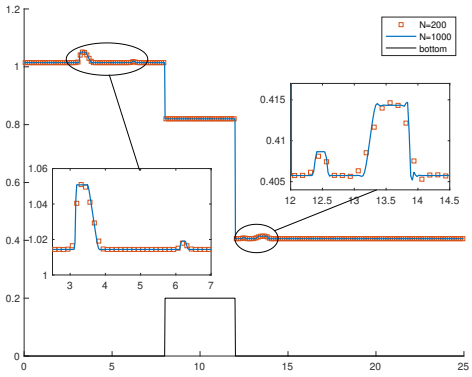

(c) Case (c)

Figure 2: Surface level $h+\phi$ and bottom in the test of small perturbations of steady states for discontinuous bottom in Example 4.5.

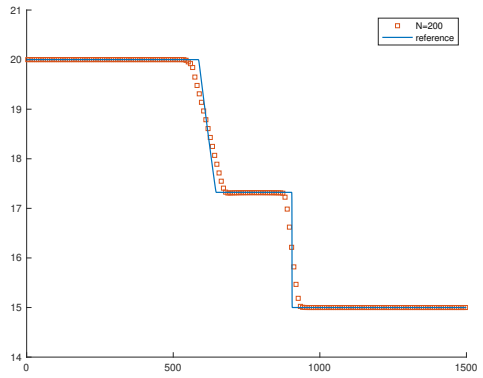

(a) $N = 200, T = 15$

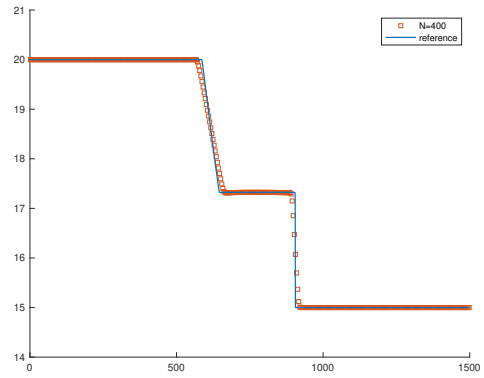

(b) $N = 400, T = 15$

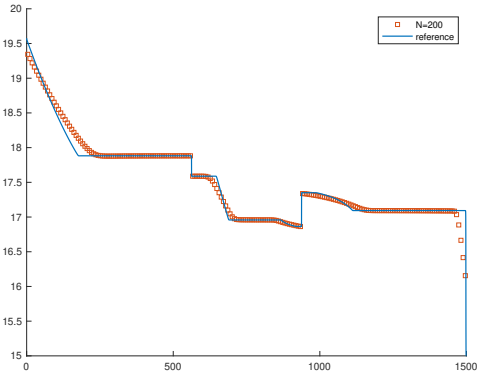

(c) $N = 200, T = 60$

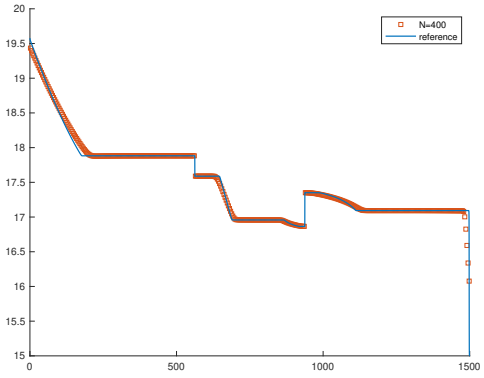

(d) $N = 400, T = 60$

Figure 3: Surface level $h + \phi$ of the dam breaking problem 4.6.

4.2 The Euler equations

Example 4.7. ***Accuracy test***

In this example, we test the accuracy of the proposed well-balanced DG method for the Euler equations in a gravitational field.

We take the linear gravitational field $\phi(x) = x$ *and ratio of specific heat* $\gamma = \frac{5}{3}$*. An exact solution of the Euler equations* (1.5) *is then given by*

$$\rho(x,t) = 1 + \frac{1}{5}\sin(\pi(x - u_0 t)), \quad u(x,t) = u_0, \quad p(x,t) = p_0 + u_0 t - x + \frac{1}{5\pi}\cos(\pi(x - u_0 t)), \tag{4.4}$$

in the domain $\Omega = [0, 2]$*, where* u_0*,* p_0 *are constants taken as* $u_0 = 1, p_0 = 4.5$ *in the computation.*

The L^1 *errors and orders of convergence of* ρ, m *and* E *are listed in Table 4 at the terminal time* $T = 0.1$*, where we can clearly observe the optimal convergence rates for* P^1*,* P^2 *and* P^3*-DG methods.*

Example 4.8. ***Well-balanced test***

In this example, we test the well-balanced property of the proposed scheme for steady-state isentropic flows.

We take the gravitational filed $\phi(x) = x$ *and ratio of specific heat* $\gamma = \frac{5}{3}$*, with the initial conditions satisfying*

$$s(x,0) = 1, \quad m(x,0) = -M\gamma^{\frac{1}{2}}, \quad Q(x,0) = \frac{1}{2}M^2\gamma + \frac{\gamma}{\gamma - 1}, \tag{4.5}$$

on the domain $\Omega = [0, 2]$*. The boundary conditions are imposed by keeping constant values that equal the initial conditions.*

Below, we consider three equilibria in different flow regimes:

(a) Hydrostatic flow: $M = 0$*.*

(b) Subcritical flow: $M = 0.01$*.*

(c) Supercritical flow: $M = 2.5$*.*

We compute the solutions up to $t = 10$ *on* $N = 200$ *uniform meshes, and gather the* L^1 *and* L^∞ *errors compared with the initial conditions in Table 5, from which we can observe the steady states are exactly preserved up to round-off errors.*

Example 4.9. ***Small perturbation of steady states***

In this example, we test the capability of the scheme to capture small perturbations of equilibria.

		ρ		m		E	
P^k-DG	N	L^1 error	order	L^1 error	order	L^1 error	order
	20	2.25E-03	-	2.61E-03	-	2.05E-03	-
	40	5.33E-04	2.08	6.18E-04	2.08	4.79E-04	2.10
$k=1$	80	1.32E-04	2.02	1.51E-04	2.03	1.16E-04	2.05
	160	3.28E-05	2.01	3.75E-05	2.01	2.84E-05	2.02
	320	8.18E-06	2.00	9.35E-06	2.00	7.04E-06	2.01
	20	1.25E-04	-	1.35E-04	-	6.35E-05	-
	40	1.66E-05	2.91	1.77E-05	2.94	8.57E-06	2.89
$k=2$	80	2.12E-06	2.97	2.21E-06	3.00	1.10E-06	2.96
	160	2.65E-07	3.00	2.73E-07	3.02	1.39E-07	2.99
	320	3.30E-08	3.01	3.37E-08	3.01	1.74E-08	3.00
	20	6.95E-07	-	6.45E-07	-	1.20E-06	-
	40	4.15E-08	4.07	4.25E-08	3.92	6.12E-08	4.29
$k=3$	80	3.03E-09	3.78	3.00E-09	3.82	3.84E-09	4.00
	160	2.13E-10	3.83	2.16E-10	3.80	2.34E-10	4.04
	320	1.36E-11	3.97	1.38E-11	3.96	1.51E-11	3.96

Table 4: L^1 errors and orders of convergence in the accuracy test 4.7 for the Euler equations.

	ρ		m		E	
Case	L^1 error	L^∞ error	L^1 error	L^∞ error	L^1 error	L^∞ error
(a)	5.53E-15	1.70E-14	7.30E-16	1.95E-15	1.13E-15	3.11E-15
(b)	4.52E-15	1.24E-14	8.51E-16	2.05E-15	1.28E-15	3.77E-15
(c)	1.15E-14	1.20E-14	1.90E-14	1.95E-14	3.40E-14	3.46E-14

Table 5: L^1 and L^∞ errors for different cases in the well-balanced test 4.8 with $N = 200$ at $T = 10$. Case (a): $M = 0$; Case (b): $M = 0.01$; Case (c): $M = 2.5$.

We add $\delta p = A\exp(-100(x-\bar{x})^2)$ *on top of the initial pressure of case (a), (b) and (c) in Example 4.8, and keep density and velocity the same as before, where* $A = 10^{-6}$ *and*

$$\bar{x} = \begin{cases} 1.0, & \textit{case (a)}, \\ 1.1, & \textit{case (b)}, \\ 1.5, & \textit{case (c)}. \end{cases}$$

We compute the solutions up to $t = 0.45, 0.45$ *and* 0.25 *for the case (a), (b) and (c), respectively. The discrepancy of pressure and velocity with respect to their corresponding base steady states are shown in Figure 4, together with the results of a non-well-balanced DG scheme with the straightforward approximation of source term and normal OFDG damping term for comparison. We can see the well-balanced scheme captures small perturbations much better than the non-well-balanced scheme on coarse meshes.*

Example 4.10. ***Discontinuous wave propogation***

In this example, we test the capability of the proposed scheme to capture shocks and large gradients of solutions. We enlarge the perturbation in Example 4.9 by taking $A = 1$ *in the pressure deviation* δp *therein, with all other parameters kept the same.*

The numerical results of the well-balanced scheme are shown in Figure 5, and are compared with those of the non-well-balanced scheme with a straightforward approximation of source terms and normal OFDG damping term. The reference solutions are computed by the WENO finite difference scheme on $N = 6400$ *mesh. We can see the well-balanced scheme and non-well-balanced scheme produce indistinguishable solutions with essentially oscillation free fashion as expected, and agree very well with those of the WENO schemes on the fine mesh. We noticed two times larger OFDG damping coefficients than the ones proposed in [29] is needed in the computation of case (b), for both the well-balanced and non-well-balanced DG schemes, to avoid negative pressure. This is possibly because of the low pressure near the right boundary.*

5 Concluding remarks

In this paper, we have established a high order well-balanced discontinuous Galerkin method for the non-hydrostatic equilibria of the shallow water equations and Euler equations. The well-balanced property is achieved through a special reformulation of the source term to mimic the flux gradient. Subsequently, the source term integral is discretized at Gauss-Lobatto points to cancel the flux integral evaluated by the

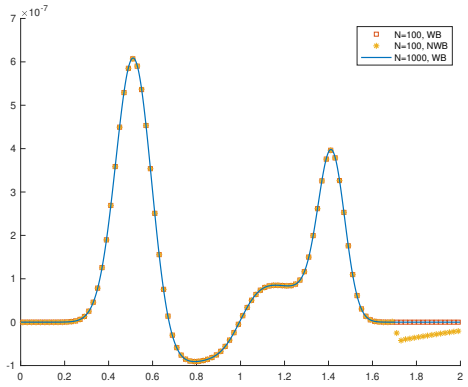

(a) Discrepancy of pressure in case (a)

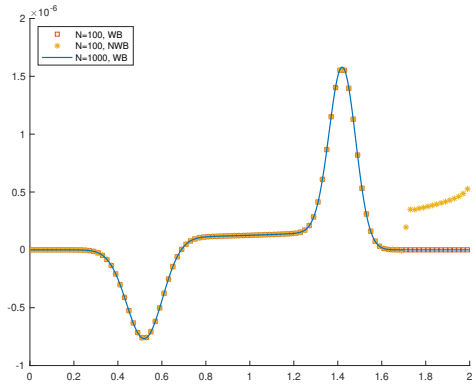

(b) Discrepancy of velocity in case (a)

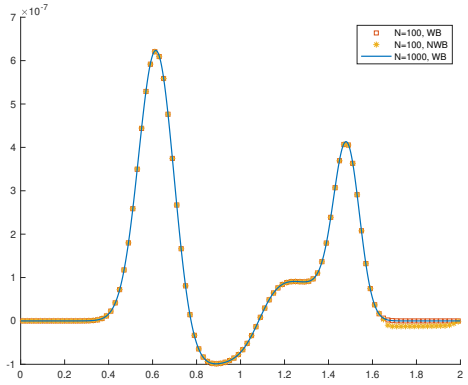

(c) Discrepancy of pressure in case (b)

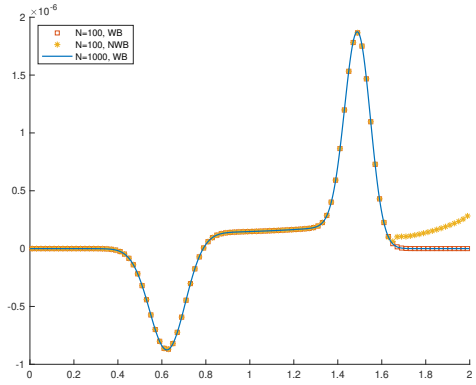

(d) Discrepancy of velocity in case (b)

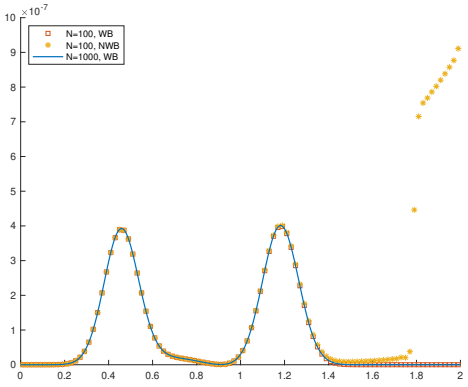

(e) Discrepancy of pressure in case (c)

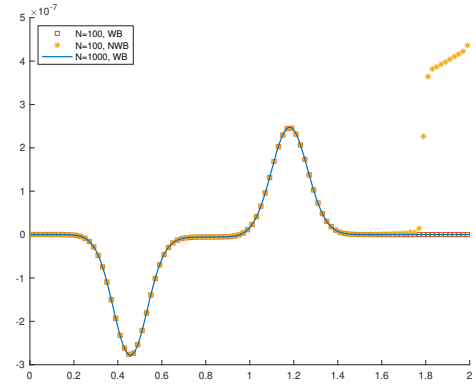

(f) Discrepancy of velocity in case (c)

Figure 4: Discrepancy of pressure and velocity with respect to their base steady states in small perturbation test 4.9. WB: well-balanced scheme; NWB: non-well-balanced scheme.

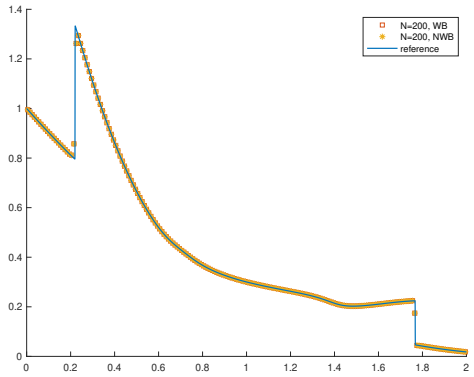

(a) Pressure in case (a)

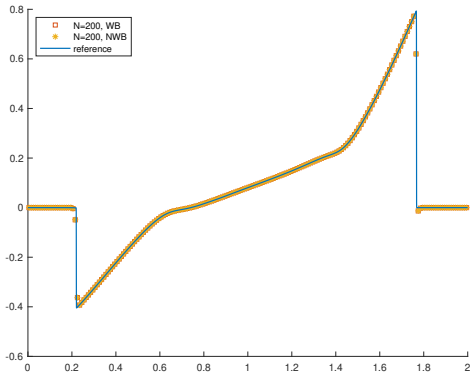

(b) Velocity in case (a)

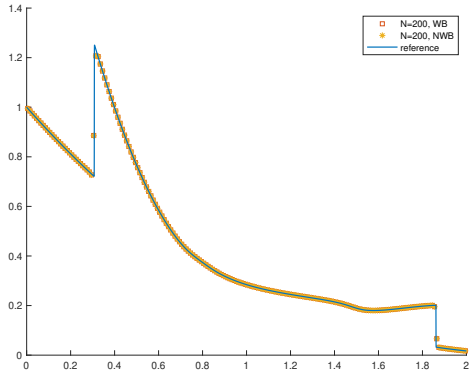

(c) Pressure in case (b)

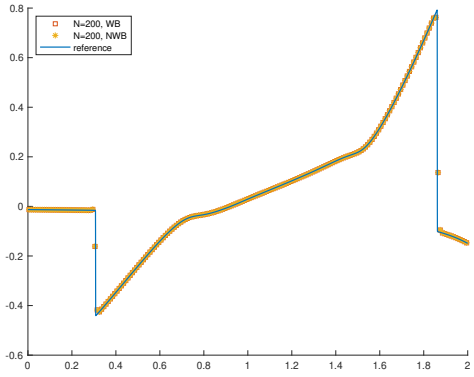

(d) Velocity in case (b)

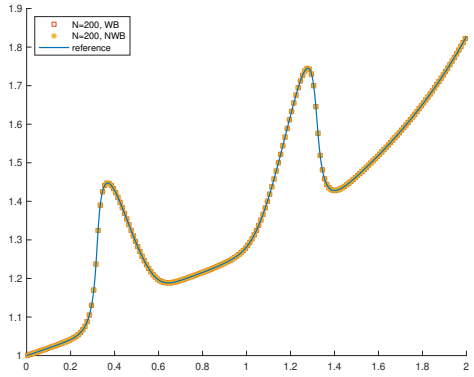

(e) Pressure in case (c)

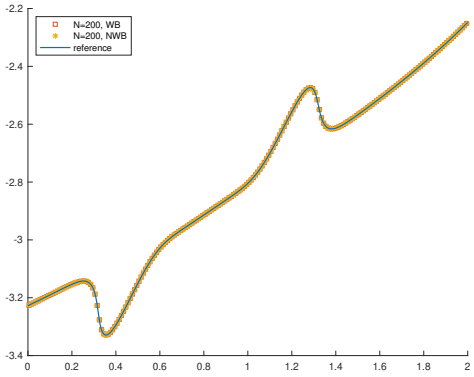

(f) Velocity in case (c)

Figure 5: Pressure and velocity in discontinuous wave propogation test 4.10.

Gauss-Lobatto quadrature and the numerical fluxes. A modified OFDG damping term is added to the scheme to control spurious oscillations near shocks without breaking the well-balanced property. Though the non-hydrostatic equilibria are generally non-polynomials, the steady states are exactly preserved at all Gauss-Lobatto points by the scheme, if the initial conditions are obtained from Lagrange interpolation at Gauss-Lobatto points. As verified by ample numerical tests, the scheme is high-order accurate, well-balanced, and capable of capturing small perturbations of steady states and shocks well.

References

[1] E. Audusse, F. Bouchut, M.-O. Bristeau, R. Klein, and B. Perthame, A fast and stable well-balanced scheme with hydrostatic reconstruction for shallow water flows, SIAM Journal on Scientific Computing, 25, 2004, 2050-2065.

[2] A. Bermudez and M. E. Vazquez, Upwind methods for hyperbolic conservation laws with source terms, Computers & Fluids, 23, 1994, 1049-1071.

[3] F. Bouchut and T.M. De Luna, A subsonic-well-balanced reconstruction scheme for shallow water flows, SIAM Journal on Numerical Analysis, 48, 2010, 1733-1758.

[4] J. Britton and Y. Xing, High order still-water and moving-water equilibria preserving discontinuous Galerkin methods for the Ripa model, Journal of Scientific Computing, 82, 2020, 1-37.

[5] M. Castro, J. Gallardo and C. Parés, High order finite volume schemes based on reconstruction of states for solving hyperbolic systems with nonconservative products. Applications to shallow-water systems, Mathematics of Computation, 75, 2006, 1103-1134.

[6] P. Chandrashekar and M. Zenk, Well-balanced nodal discontinuous Galerkin method for Euler equations with gravity, Journal of Scientific Computing, 71, 2017, 1062-1093.

[7] Y. Cheng, A. Chertock, M. Herty, A. Kurganov, and T. Wu, A new approach for designing moving-water equilibria preserving schemes for the shallow water equations, Journal of Scientific Computing, 80, 2019, 538-554.

[8] Y. Cheng and A. Kurganov, Moving-water equilibria preserving central-upwind schemes for the shallow water equations, Communications in Mathematical Sciences, 14, 2016, 1643-1663.

[9] B. Cockburn, S. Hou and C.-W. Shu, The Runge-Kutta local projection discontinuous Galerkin finite element method for conservation laws IV: the multidimensional case, Mathematics of Computation, 54, 1990, 545-581.

[10] B. Cockburn, S.-Y. Lin and C.-W. Shu, TVB Runge-Kutta local projection discontinuous Galerkin finite element method for conservation laws III: one-dimensional systems, Journal of Computational Physics, 84, 1989, 90-113.

[11] B. Cockburn and C.-W. Shu, TVB Runge-Kutta local projection discontinuous Galerkin finite element method for conservation laws II: general framework, Mathematics of Computation, 52, 1989, 411-435.

[12] B. Cockburn and C.-W. Shu, The Runge-Kutta local projection P1-discontinuous-Galerkin finite element method for scalar conservation laws, ESAIM: Mathematical Modelling and Numerical Analysis, 25, 1991, 337-361.

[13] B. Cockburn and C.-W. Shu, The Runge–Kutta discontinuous Galerkin method for conservation laws V: multidimensional systems, Journal of Computational Physics, 141, 1998, 199-224.

[14] I. Gómez-Bueno, M. Castro and C. Parés, High-order well-balanced methods for systems of balance laws: a control-based approach, Applied Mathematics and Computation, 394, 2021, 125820.

[15] L. Grosheintz-Laval and R. Käppeli, High-order well-balanced finite volume schemes for the Euler equations with gravitation, Journal of Computational Physics, 378, 2019, 324-343.

[16] L. Grosheintz-Laval and R. Käppeli, Well-balanced finite volume schemes for nearly steady adiabatic flows, Journal of Computational Physics, 423, 2020, 109805.

[17] J.S. Hesthaven and T. Warburton, Nodal discontinuous Galerkin methods: algorithms, analysis, and applications, Springer, 2007.

[18] R. Käppeli, Well-balanced methods for computational astrophysics, Living Reviews in Computational Astrophysics, 8, 2022, 2.

[19] R. Käppeli and S. Mishra, Well-balanced schemes for the Euler equations with gravitation, Journal of Computational Physics, 259, 2014, 199-219.

[20] C. Klingenberg, A. Kurganov, and M. Zenk, Moving-water equilibria preserving HLL-type schemes for the shallow water equations, Commun. Math. Res., 36, 2020, 247-271.

[21] C. Klingenberg, G. Puppo, and M. Semplice, Arbitrary order finite volume well-balanced schemes for the Euler equations with gravity, SIAM Journal on Scientific Computing, 41, 2019, A695-A721.

[22] A. Kurganov and D. Levy, Central-upwind schemes for the Saint-Venant system, ESAIM: Mathematical Modelling and Numerical Analysis, 36, 2002, 397-425.

[23] A. Kurganov and G. Petrova, A second-order well-balanced positivity preserving central-upwind scheme for the Saint-Venant system, Communications in Mathematical Sciences, 5, 2007, 133-160.

[24] W.D. Lambert, A generalized trigonometric solution of the cubic equation, The American Mathematical Monthly, 13, 1906, 73-76.

[25] G. Li and Y. Xing, High order finite volume WENO schemes for the Euler equations under gravitational fields, Journal of Computational Physics, 316, 2016, 145-163.

[26] G. Li and Y. Xing, Well-balanced discontinuous Galerkin methods with hydrostatic reconstruction for the Euler equations with gravitation, Journal of Computational Physics, 352, 2018, 445-462.

[27] G. Li and Y. Xing, Well-balanced finite difference weighted essentially non-oscillatory schemes for the Euler equations with static gravitational fields, Computers & Mathematics with Applications, 75, 2018, 2071-2085.

[28] X. Liu, X. Chen, S. Jin, A. Kurganov, T. Wu, and H. Yu, Moving-water equilibria preserving partial relaxation scheme for the Saint-Venant system, SIAM Journal on Scientific Computing, 42, 2020, A2206-A2229.

[29] Y. Liu, J. Lu and C.-W. Shu, An essentially oscillation-free discontinuous Galerkin method for hyperbolic systems, SIAM Journal on Scientific Computing, 44, 2022, A230-A259.

[30] Y. Liu, J. Lu, Q. Tao and Y. Xia, An oscillation-free discontinuous Galerkin method for shallow water equations, Journal of Scientific Computing, 92, 2022, 109.

[31] Y. Mantri and S. Noelle, Well-balanced discontinuous Galerkin scheme for 2×2 hyperbolic balance law, Journal of Computational Physics, 429, 2021, 110011.

[32] S. Noelle, N. Pankratz, G. Puppo, and J.R. Natvig, Well-balanced finite volume schemes of arbitrary order of accuracy for shallow water flows, Journal of Computational Physics, 213, 2006, 474-499.

[33] S. Noelle, Y. Xing, and C.-W. Shu, High-order well-balanced finite volume WENO schemes for shallow water equation with moving water, Journal of Computational Physics, 226, 2007, 29-58.

[34] C. Parés and C. Parés-Pulido, Well-balanced high-order finite difference methods for systems of balance laws, Journal of Computational Physics, 425, 2021, 109880.

[35] W.H. Reed and T.R. Hill, Triangular mesh methods for the neutron transport equation, Los Alamos Scientific Laboratory, 1973.

[36] R. Touma, U. Koley, and C. Klingenberg, Well-balanced unstaggered central schemes for the Euler equations with gravitation, SIAM Journal on Scientific Computing, 38, 2016, B773-B807.

[37] M.E. Vázquez-Cendón, Improved treatment of source terms in upwind schemes for the shallow water equations in channels with irregular geometry, Journal of Computational Physics, 148, 1999, 497-526.

[38] K. Wu and Y. Xing, Uniformly high-order structure-preserving discontinuous Galerkin methods for Euler equations with gravitation: Positivity and well-balancedness, SIAM Journal on Scientific Computing, 43, 2021, A472-A510.

[39] Y. Xing, Exactly well-balanced discontinuous Galerkin methods for the shallow water equations with moving water equilibrium, Journal of Computational Physics, 257, 2014, 536-553.

[40] Y. Xing and C.-W. Shu, High order finite difference WENO schemes with the exact conservation property for the shallow water equations, Journal of Computational Physics, 208, 2005, 206-227.

[41] Y. Xing and C.-W. Shu, High order well-balanced finite volume WENO schemes and discontinuous Galerkin methods for a class of hyperbolic systems with source terms, Journal of Computational Physics, 214, 2006, 567-598.

[42] Y. Xing and C.-W. Shu, A new approach of high order well-balanced finite volume WENO schemes and discontinuous Galerkin methods for a class of hyperbolic systems with source terms, Communications in Computational Physics, 1, 2006, 100-134.

[43] Y. Xing and C.-W. Shu, High order well-balanced WENO scheme for the gas dynamics equations under gravitational fields, Journal of Scientific Computing, 54, 2013, 645-662.

[44] Z. Xu and C.-W. Shu, A high-order well-balanced alternative finite difference WENO (A-WENO) method with the exact conservation property for systems of hyperbolic balance laws, submit for review.

[45] J. Zhang, Y. Xia, and Y. Xu, Moving water equilibria preserving discontinuous Galerkin method for the shallow water equations, Journal of Scientific Computing, 95, 2023, 48.